Microstructural differences in white matter tracts across middle-to-late adulthood: A diffusion MRI study on 7167 UK Biobank participants

Wen-Yih Isaac Tseng, Yung-Chin Hsu, Chang-Le Chen, Yun-Jing Kang, Te-Wei Kao, Pin-Yu Chen, Gordon D. Waiter

Author Affiliations:

Institute of Medical Device and Imaging, National Taiwan University College of Medicine, Taipei, Taiwan (Tseng, Kang, Kao, Chen, Chen);

Acroviz Technology Inc. Taipei, Taiwan (Hsu);

Molecular Imaging Center, National Taiwan University, Taipei, Taiwan (Tseng);

Aberdeen Biomedical Imaging Centre, School of Medicine, Medical Sciences and Nutrition, University of Aberdeen (Waiter).

Corresponding Author: Gordon D. Waiter, Aberdeen Biomedical Imaging Centre

School of Medicine, Medical Sciences and Nutrition, University of Aberdeen, Lilian Sutton Building, Foresterhill, Aberdeen, AB25 2ZD, UK. Tel: +44 (0)1224 438356 (University Internal 8356: NHS Internal 768356); Fax: +44 (0)1224 438364; Email: g.waiter@abdn.ac.uk

Abstract

White matter fiber tracts demonstrate heterogeneous vulnerabilities to aging effects. Here, we estimated age-related differences in tract properties using UK Biobank diffusion magnetic resonance imaging (dMRI) data of 7167 47–76-year-old neurologically healthy people (3368 men and 3799 women). Tract properties in terms of generalized fractional anisotropy (GFA), axial diffusivity (AD), radial diffusivity (RD), and mean diffusivity (MD), were sampled on 76 fiber tracts; for each tract, age-related differences were estimated by fitting these indices against age in a linear model. This cross-sectional study demonstrated four age-difference patterns. The dominant pattern was lower GFA and higher AD, RD, and MD with age, constituting 45 of 76 tracts, mostly involving the association, projection and commissure fibers connecting the prefrontal lobe. The other three patterns constituted only 14 tracts, with atypical age differences in diffusion indices, and mainly involved parietal, occipital, and temporal cortices. By analyzing the large volume of dMRI data available from the UK Biobank, the study has provided a detailed description of heterogeneous age-related differences in tract properties over the whole brain which generally supports the myelodegeneration hypothesis.

1. Introduction

1.1. Axons, connectomics, and cognitive functions

Cognitive functions of the brain are regulated by finely tuned signal transmission between connected neurons (Ackman et al., 2012). Recent advances in connectomics have rekindled the research interest in hodology by emphasizing the importance of connections between neurons for proper cognitive function (Hagmann et al., 2008). Neurons are interconnected by neuronal axons, which provide structural support for functional connectivity from the microscopic to macroscopic levels (Sporns et al., 2005). Studies on diffusion magnetic resonance imaging (dMRI) have reported that the microstructural properties of white matter (WM) fiber tracts are associated with cognitive functions in both normal and diseased brains (Antonenko and Floel, 2014; Wallace et al., 2018). Even during normal aging, alterations in dMRI indices with age have been found to be associated with cognitive decline (Bennett and Madden, 2014).

1.2. Patterns of dMRI-derived tract properties as a potential biomarker

Aging effects on axonal fibers may occur at least one decade before manifestation of overt symptoms of cognitive decline (Araque Caballero et al., 2018). If brain pathology is involved, the associated fiber alterations present on top of the alterations caused by normal aging (Seltzer et al., 2004). Therefore, an accurate description of the alteration patterns related to normal aging is required to differentiate them from pathological alterations (Fjell et al., 2014). Through comparison with the standard patterns of tract alteration due to normal aging, any deviation in tract alteration can be detected. Furthermore, different neurodegenerative diseases may present different patterns of tract alteration early in the course of disease, which might serve as biomarkers for risk prediction or therapeutic monitoring.

1.3. WM fiber tracts in neuroimaging of the aging brain

dMRI is the only noninvasive imaging modality that can be used to probe WM fiber tract properties in vivo (Beaulieu, 2002). Diffusion signals measured using dMRI reflect the geometric property of the underlying microstructure. Diffusion tensor imaging (DTI) is a widely used dMRI technique, in which the diffusion phenomenon is modeled as a three-dimensional (3D) Gaussian function of displacement probability (Basser et al., 1994). By fitting the Gaussian function as a rank-2 tensor, scalar indices can be extracted to obtain different diffusivity features of the probed microstructure. The most commonly used diffusion indices include axial diffusivity (AD), radial diffusivity (RD), mean diffusivity (MD), and fractional anisotropy (FA). AD refers to the first eigenvalue corresponding to the first eigenvector of the diffusion tensor, and RD refers to the mean of the second and third eigenvalues. MD is determined by averaging the three eigenvalues of the diffusion tensor, and FA indicates the degree of anisotropy of the diffusion tensor. Many studies have used DTI to study alterations of fiber property in normally aged brains or in brains of those with neurodegenerative diseases (Gold and Keller, 2012). However, most studies have been limited by small sample sizes or focus on limited numbers of regions or diffusion indices, thus limiting the generalizability of the results (Chen-Plotkin, 2014). Recently, Cox et al. analyzed brain MRIs of 3513 generally healthy people from the UK Biobank cohort using both conventional DTI and newly developed diffusion metrics in 27 major white matter tracts (Cox et al., 2016). To delineate spatial heterogeneity of dMRI-derived tract properties in more detail, specifically which tracts are vulnerable or resilient to aging effects, more UK Biobank participants are desirable to analyze age-related differences in all four DTI indices on more refined tracts.

1.4. Opportunities for mapping heterogeneous aging effects on WM fiber tracts in normal aging

The dMRI data from the UK Biobank could enable the development of spatial patterns of dMRI-derived tract properties in normal aging. Up to the date of the current study, the UK Biobank released approximately 9000 dMRI datasets. To convert such large amounts of dMRI raw data to information on tract-specific property is challenging. An automatic pipeline comprising data screening, diffusion tensor reconstruction, quality assurance, image registration, and tract-specific analysis must be developed. We recently developed a tract-based automatic analysis (TBAA) technique and established a complete processing pipeline for dMRI data (Chen et al., 2015). Thus far, the TBAA technique and processing pipeline have been applied in clinical studies on various neurological or psychiatric diseases (Chen et al., 2018; Chien et al., 2017; Huang et al., 2018; Lo et al., 2019; Tsai et al., 2019; Wu et al., 2015). By using massive dMRI data provided by the UK Biobank and our automatic analysis pipeline, we aimed to characterize heterogeneous patterns of age-related differences in dMRI-derived tract properties in healthy individuals aged 47–76 years.

1.5. Purpose of the study

The purpose of this cross-sectional design study was to characterize spatial patterns of dMRI-derived tract properties in normal aging and provide detailed sex-stratified data for each fiber tract and each diffusion index. To account for the heterogeneity in dMRI-derived tract properties, we described the patterns of age-related differences in tract properties at 5 levels of fiber tract grouping, including the whole brain, three fiber systems, and individual fiber tracts. In particular, we described the patterns in terms of the four aforementioned diffusion indices, namely FA, AD, RD, and MD, and their corresponding spatial distributions. With the brain-wide view of age-related differences in tract properties, we aimed to test whether the heterogeneous spatial pattern supports the myelodegeneration hypothesis (Bartzokis, G., 2004; Davis et al., 2009), i.e. late-myelinating white matter tracts show earlier declines.

2. Methods

2.1. Data source

2.1.1. Participants

The UK Biobank prospectively contains extensive health-related data of a cohort of 500,000 participants, including questionnaires, physical and cognitive measures, and biological samples (Miller et al., 2016). Participants were in their fifth to eighth decade of age at baseline recruitment. The total number of recruited male and female participants up to September 2017 was 238,720 and 263,908, respectively (Sudlow et al., 2015). In 2014, an imaging extension was initiated with the aim of scanning 100,000 participants. The first imaging center was built in Cheadle, Greater Manchester, England, where approximately 2% of the participants underwent scanning over a 2-year ramp-up period. Of this group 8830 had usable T1-weighted (T1w) MRI, T2-FLAIR, and dMRI data. Details of unusable MRI data are presented in Supplementary Text 1.

2.1.2. MRI data acquisition

MRI scanning was performed using 3T Siemens Skyra System (Siemens, Erlangen, Germany) with the VD13A SP4 operating system and a 32-channel RF receiver head coil. T1wimages were acquired using a 3D magnetization-prepared rapid gradient-echo pulse sequence under the following conditions: Inversion time (TI)/repetition time (TR) = 880/2000 ms, field-of-view (FOV) = 208 × 256 × 256 mm^3, resolution= 1 × 1 × 1 mm^3, sagittal plane, and in-plane acceleration factor = 2. T2-FLAIR images were acquired using 3D sampling perfection with application-optimized contrasts with fat saturation under the following conditions: TI/TR = 1800/5000ms, FOV = 192×256×256 mm^3, resolution = 1.05×1×1 mm^3, sagittal plane, and in-plane acceleration factor =2. dMRI was conducted using a standard (monopolar) spin-echo echo-planar imaging sequence with 5 baseline images (b = 0 s mm^{-2}), 50 diffusion-weighted images with b = 1000 s mm^{-2}, and 50 diffusion-weighted images with b = 2000 s mm^{-2} with the following imaging parameters: TR/TE = 3600/92 ms, FOV = 104 × 104 mm^2, in-plane resolution = 2 ×2 mm^2, slice thickness = 2 mm, slice number = 72, transaxial plane, and multislice acceleration = 3. In addition to the primary dMRI data, 3 b=0s mm^{-2} images with reversed phase encoding were acquired for subsequent field map estimation along with 3 b=0s mm^{-2} images with standard phase encoding. The estimated field map was used for distortion correction in the dMRI datasets.

2.2. Data screening

To ensure that participants who underwent scanning were neurologically healthy, participants with a history of neurological or psychiatric disease, substance abuse, and malignancy (as listed in Supplementary Text 1) or an IQ outside the range 100±30 (mean±2 SD) were excluded from the analysis. We also excluded imaging data with poor quality, including images with a poor signal-to-noise ratio, failed distortion correction, or large intrascanning displacement between dMRI and T1w images, and incomplete imaging data. Finally, after data screening, data of 7692 participants, including 3653 men and 4039 women, were eligible for inclusion.

2.3. Image processing

2.3.1. Reconstruction of dMRI data

For each participant, the TOPUP tool (Andersson et al., 2003) was applied on the b=0 s mm^{-2} dMRI images with opposite phase-encoding direction to estimate the b = 0 field map. The EDDY tool (Andersson and Sotiropoulos, 2015; Andersson and Sotiropoulos, 2016) was then applied on the primary dMRI dataset to correct for susceptibility-induced distortions, eddy current–induced distortions, head motion, and outlier slices (individual slices in the 4D data).

In this study, we employed the mean apparent propagator (MAP)-MRI algorithm (Ozarslan et al., 2013) to process the diffusion signals. MAP-MRI is a generalization of DTI which models the signal profiles as a linear combination of Hermite functions. MAP-MRI has a sound theoretical framework and great generalizability to various diffusion acquisition schemes. In practice, the diffusion data (both shells) was fitted to a diffusion tensor model which includes the Gaussian function and also the zero-order Hermite functions. Tensor estimation was conducted using the approach proposed in Koay et al. (2006). Specifically, the weighted linear least-squares method was used to generate an initial estimation of the tensor, which served as a starting point of a nonlinear least-squares method. The resultant tensor of the nonlinear least-squares algorithm was positive-definite as a positivity constraint was imposed during estimation (Koay et al., 2006)). The higher-order terms, which are the orthogonal corrections to the Gaussian approximation and account for the non-Gaussian components of the diffusion signals, were subsequently obtained from the fitted Hermite functions. Because Fourier transforms of the Hermite functions are also Hermite functions, the diffusion propagator and orientation distribution function (ODF) were reconstructed from the estimated coefficients. Ning et al. (Ning et al., 2015) used a physical phantom to comprehensively compare several reconstruction algorithms, including constrained spherical deconvolution and MAP-MRI. The results revealed that among the reconstruction algorithms, the MAP-MRI method provided the most accurate reconstruction, with a low normalized mean square error and low percentage of false peaks.

From the ODF, the generalized fractional anisotropy (GFA) (Tuch, 2004), which is analogous to FA in DTI, was calculated. The diffusivity indices MD, RD, and AD were calculated as defined in the DTI model. These indices have been considered surrogate markers for different microstructural properties of WM (Alexander et al., 2011). Other diffusion indices from MAP-MRI such as return-to-the-origin probability, return-to-the-axis probability, return-to-the-plane probability, non-Gaussianity, non-Gaussianity along the principal eigenvector, and non-Gaussianity perpendicular to the principal eigenvector were not reported in this paper because they are not fully characterized and their associations with microstructural correspondence remain unclear. Diffusion data reconstructions, including DTI estimation, MAP-MRI estimation, and diffusion index calculation, were processed using in-house programs written using MATLAB (The MathWorks, Inc., Natick, MA, USA).

2.3.2. Tract-based analysis of diffusion indices

In this study, we employed TBAA to avoid intra-rater and inter-rater variability and the potential errors from human factors in tract-specific analysis of dMRI data. To perform diffusion index sampling along each of the fiber tracts, TBAA was conducted to sample the diffusion indices from 76 predefined major fiber tract bundles over the whole brain (Chen et al., 2015). These 76 major fiber tract bundles were previously reconstructed in NTU-DSI-122, a DSI template, through deterministic streamline-based tractography, with multiple regions of interest defined in the automated anatomical labeling atlas (Lyttelton et al., 2007). NTU-DSI-122 comprises DSI datasets from 122 healthy adults; these data sets are registered in the ICBM-152 space (Hsu et al., 2015). The dMRI images and T1w images from the UK Biobank were registered in NTU-DSI-122-DTI, a DTI template previously derived from NTU-DSI-122 template (available at http://www.nitrc.org/projects/ntu-dsi-122/). After registration, the coordinates of the 76 tracts were transformed from the ICBM-152 space to the individual native space with corresponding deformation maps. The deformation maps were obtained through a group-wise registration, which included anatomical information obtained from the T1w images and microstructural information obtained from the diffusion datasets. The group-wise registration process comprised two steps involving the Shoot algorithm (Ashburner and Friston, 2011) of SPM12 and the LDDMM-DTI method (Cao et al., 2006) implemented in-house. Detailed procedures of the registration and validation of the registration accuracy are described in Supplementary Text 2 and Supplementary Fig. 1. Figure 1 shows the tractogram of 76 white matter fiber tracts in the DSI template.

Fig. 1. Tractogram of the 76 white matter tracts in the DSI template. Please see Supplementary Table 1 for the full names of the tracts.

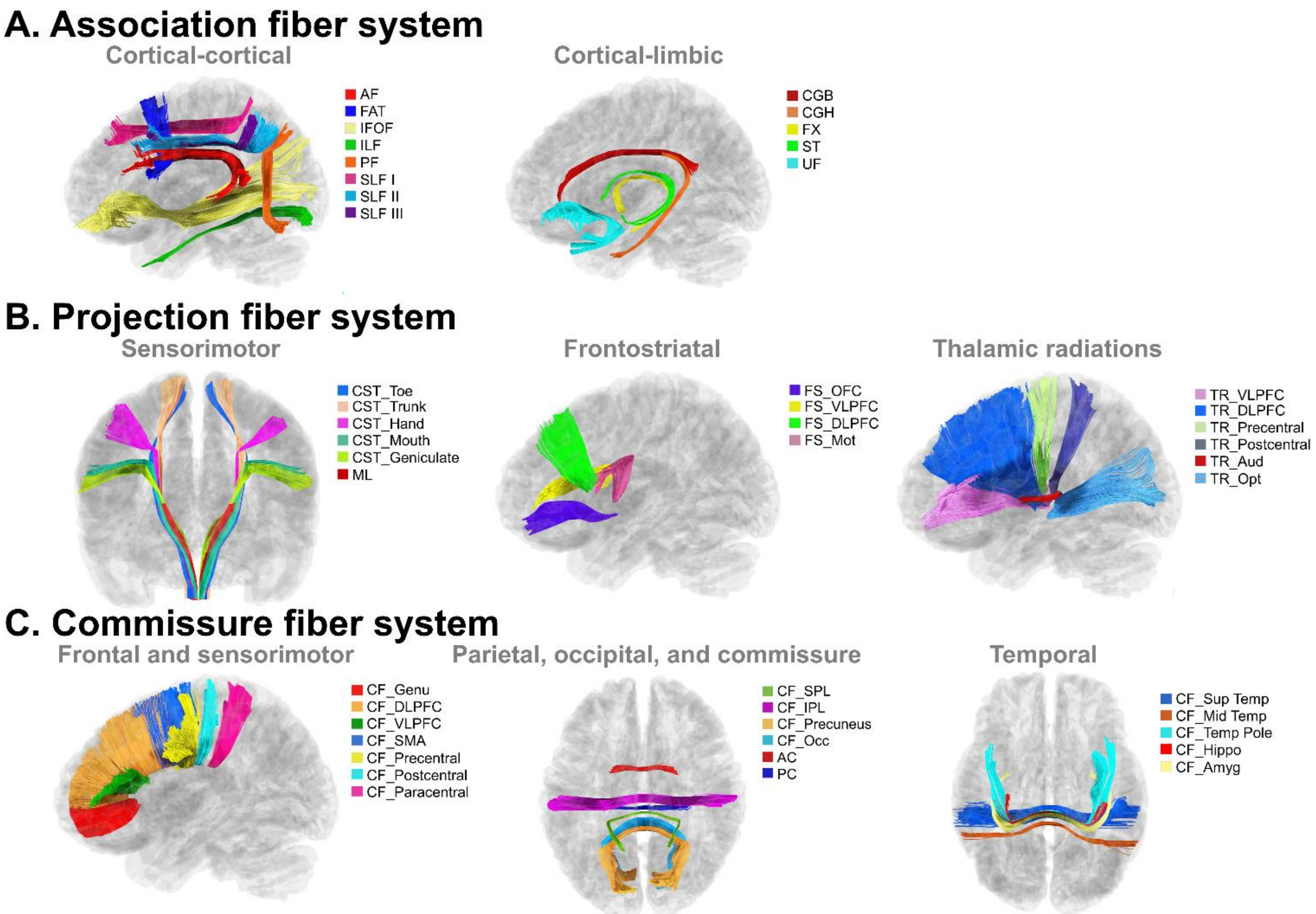
A. Association fiber system
Cortical-cortical
AF
FAT
IFOF
ILF
PF
SLF I
SLF II
SLF III
Cortical-limbic
CGB
CGH
FX
ST
UF
B. Projection fiber system
Sensorimotor
CST_Toe
CST_Trunk
CST_Hand
CST_Mouth
CST_Geniculate
ML
Frontostriatal
FS_OFC
FS_VLPFC
FS_DLPFC
FS_Mot
Thalamic radiations
TR_VLPFC
TR_DLPFC
TR_Precentral
TR_Postcentral
TR_Aud
TR_Opt
C. Commissure fiber system
Frontal and sensorimotor
CF_Genu
CF_DLPFC
CF_VLPFC
CF_SMA
CF_Precentral
CF_Postcentral
CF_Paracentral
Parietal, occipital, and commissure
CF_SPL
CF_IPL
CF_Precuneus
CF_Occ
AC
PC
Temporal
CF_Sup Temp
CF_Mid Temp
CF_Temp Pole
CF_Hippo
CF_Amyg

Each fiber tract bundle was divided into 100 equal steps, and the diffusion indices were sampled in the native space along the step coordinates. The output of tract-based analysis for each participant was a two-dimensional (2D) array of the sampled diffusion indices (x-axis: 100 steps along sampling coordinates; y-axis: 76 WM tract bundles). Consequently, four 2D arrays of diffusion indices were obtained from each participant corresponding to GFA, AD, RD, and MD. Tract-specific diffusion indices were calculated by using the arithmetic means of the diffusion indices over 100 steps.

Image registration and tract-specific sampling were conducted using the Maxwell High Performance Computing Cluster of the University of Aberdeen IT Service (www.abdn.ac.uk/staffnet/research/hpc.php), which is provided by Dell Inc. and supported by Alces Software Ltd. and has 800 CPU cores and a total memory size of 12 TB. All in-house algorithms are proprietary owned by NTU; interested users can request WYIT (first author) for the terms of use.

2.4. Correction for cerebrospinal fluid partial volume effect

The diffusion indices at each step of the tract were confounded by the partial volume effect of CSF (PVE_{CSF}) linearly (Supplementary Fig. 2). To remove the confounding effect of PVE_{CSF}, we used the deformation maps from NTU-DSI-122-DTI to individual DTI datasets and to T1w images, tissue probabilities in the cerebrospinal fluid (CSF) derived from T1w images were sampled along each neural tract (see Supplementary Text 2), and a 100 × 76 2D array of CSF probability corresponding to PVE_{CSF} was constructed at each step along each fiber tract. This information was used to regress out PVE_{CSF} on apparent diffusion indices D_{app}. A linear regression model, $D_{app} = \beta_0 + \beta_1 \times PVE_{CSF}$, was performed on each individual by using 100×76 apparent diffusion indices and 100×76 CSF probabilities. β_1 values obtained from the regression model was used to regress out the confounding effect of PVE_{CSF} at each step of the tract, i.e. $D_{app}-\beta_1\times PVE_{CSF}$. The diffusion indices after regressing out PVE_{CSF} compared with apparent diffusion indices are detailed in Supplementary Fig. 2.

2.5. Tract grouping

To characterize spatial patterns of age-related differences, we grouped the 76 tracts into five levels: 76 tracts, 25 tract groups, 10 subsystems, 3 fiber systems, and the whole brain. The 76 tracts and their grouping are detailed in Supplementary Table 1 and Supplementary Fig. 3.

2.6. Statistical analysis

To quantify the difference in tract properties across 47–76 years of age, we used a linear regression model: $Y = \beta_0 + \beta_1\times$age, where Y denotes the mean diffusion index for each tract entity and β_1 the average annual difference. Because many tracts exhibited significant age-by-sex interactions (Supplementary Table 2), we applied the model to male and female participants separately to obtain sex-specific age difference patterns for each diffusion index. The linear regression model was used because after 45 years of age, the diffusion indices vary almost linearly with age. The justification of using the linear model rather than the quadratic model is provided in Supplementary Text 3.

The linear regression model was applied to each tract (sample, m = 76), each tract group (m = 25), each subsystem (m = 10), each fiber system (m = 3), and the whole brain (m = 1). Assuming that the tracts or tract groups within each grouping level are independent measures, Bonferroni correction was performed for multiple comparisons, and statistical significance was considered when *p* values were <0.05/m, where m was the number of comparisons within each grouping level. To characterize the spatial distributions of age-related difference in diffusion indices, $\beta_1$values that passed statistical testing were color-coded and rendered in tract maps. Tracts were ordered by 76 tracts or 25 tract groups to help appreciate the heterogeneity of age difference.

3. Results

3.1. Demographics

To ensure high-quality DTI data, we excluded participants with GFA, AD, RD, or MD in the MRI data outside the range of mean ± 4SD in any of the 76 tracts. After quality assurance, the age distribution of the diffusion index variances demonstrated no age-related bias (Supplementary Fig. 4), and 7167 participants (93.2% of 7692 people; age range, 47–76 years), including 3380 men and 3787 women, were included in the final analysis. Table 1 presents the demographic characteristics of the recruited participants.

Table 1: Demographics of participants in full sample, imaging subsample, and final subsample.

Variable	Full Sample		Imaging subsample		Final subsample	
Sex	Male	Female	Male	Female	Male	Female
N	238,720	263,908	3,653	4,039	3,380	3,787
Percentage	47.5%	52.5%	47.5%	52.5%	47.2%	52.8%
Age (years), Mean (SD)	61.47 (7.06)	61.47 (7.20)	62.77 (7.50)	61.52 (7.14)	62.41 (7.42)	61.29 (7.07)
IQ, Mean (SD)	101.4 (15.41)	98.84 (14.54)	98.25 (13.29)	100.89 (12.89)	98.14 (13.19)	100.74 (12.88)

3.2. Brain-wide patterns of age-related differences in tract properties

Age-related differences (i.e. β_1) and p values of GFA, AD, RD, and MD at five levels of tract grouping are listed in Table 2. We observed a predominant global pattern of age-related difference in diffusion indices; however, a deviation from this global pattern was observed at a more fine-grained level.

At the whole-brain level, we noted a dominant pattern of age-related difference in diffusion indices: significantly lower GFA and higher AD, RD, and MD with age (labeled in pink in Table 2). At the three-system level, the patterns were almost similar, except a nonsignificant RD difference in the commissure fiber system. At the 10-subsystem level, the pattern of lower GFA and higher AD, RD, and MD with age was seen in five subsystems. The pattern was most dominant in the association fibers, involving the limbic system and the cortico-cortical system, followed by the projection fibers, involving the frontostriatum (FS), the thalamic radiation (TR), and the least in the callosal fibers, involving the collosal fibers connecting the frontal cortex (CF_Front). In the remaining five systems, the callosal fibers connecting the temporal cortex (CF_Temp) showed an atypical pattern of higher GFA, AD and MD, and lower RD with age (labeled in orange in Table 2).

At the level of 25 tract groups, 14 tract groups exhibited the consistent global pattern. The pattern was distributed in most of the association fibers, including the body of the cingulum (CGB), the hippocampal part of the cingulum (CGH), the fornix (FX), the uncinate fasciculus (UF), the arcuate fasciculus (AF), the frontal aslant tract (FAT), the inferio-occipital fasciculus (IFOF), the inferior longitudinal fasciculus (ILF), and the superior longitudinal fasciculus (SLF). The global pattern was found in 50% of the projection fibers, including the frontostriatum of the prefrontal cortex (FS_Pfc), the frontostriatum of the motor cortex (FS_Mot), the thalamic radiation of the prefrontal cortex (TR_Pfc), and the thalamic radiation of the auditory cortex (TR_Aud). Only one part of the callosal fibers showed the global pattern, i.e. the callosal fibers connecting the sensorimotor cortex (CF_Sm). In the remaining 11 tract groups, we noted the atypical pattern of higher GFA, AD and MD, and higher /lower RD with age (labeled in orange in Table 2) in the stria terminalis (ST), the thalamic radiation of the sensorimotor cortex (TR_Sm), and CF_Temp. We also observed another atypical pattern of higher /lower GFA, lower AD, RD and MD with age (labeled in blue in Table 2) in the perpendicular fasciculus (PF), and the thalamic radiation of the optic nerve (TR_Opt).

At the level of 76 tracts, we categorized the tracts according to shared profiles of age-related difference in diffusion indices and found four main groups exhibiting distinct profiles among the 76 tracts (Table 2). The first group constituted the majority of tracts (45of 76 tracts), with higher AD, RD, and MD and lower /insignificant GFA with age (labeled in pink in Table 2). These tracts are most dominant in the association fibers (23, 88 % of 26 association fibers), followed by the projection fibers (16, 50% of 32 projection fibers), and the least in the callosal fibers (6, 33% of 18 callosal fibers). The second group comprised 8 tracts and exhibited higher AD, MD, and GFA, and higher /lower RD with age (labeled in orange in Table 2). This group included 6 projection fibers, including bilateral corticospinal tracts of the hand (CST_Hand), bilateral thalamic radiations to the precentral cortex (TR_Precentral) and bilateral postcentral cortex (TR_Postcentral), and 2 callosal fibers, namely callosal fibers connecting the superior temporal lobe (CF_Sup Temp) and posterior commissure (CF_PC). The third group comprised 4 tracts and exhibited higher GFA and AD, lower RD, and lower /insignificant MD with age (labeled in green in Table 2). These tracts included the right CST of toe (CST_Toe) and the callosal fibers connecting the middle temporal lobe (CF_Mid temp), temporal pole (CF_Temp pole), and hippocampus (CF_Hippo). The fourth group comprised 4 tracts and presented higher /lower GFA, lower AD, RD and MD with age (labeled in blue in Table 2). This group included left PF, bilateral TR_Opt and the callosal fiber connecting the ventrolateral prefrontal cortex (CF_VLPFC).

Table 2: The age-related difference in GFA, AD, RD, and MD in terms of β_1 and P values, male and female participants listed separately

$\beta_1 * 10^4$ (P-value)	GFA M	GFA F	AD $*10^{-3}$ mm^2/Sec M	AD $*10^{-3}$ mm^2/Sec F	RD$*10^{-3}$ mm^2/Sec M	RD$*10^{-3}$ mm^2/Sec F	MD$*10^{-3}$mm^2/Sec M	MD$*10^{-3}$mm^2/Sec F
Whole brain	**-1.22 (0.000)**	**-2.99 (0.000)**	**8.64 (0.000)**	**6.11 (0.000)**	**3.51 (0.000)**	**4.46 (0.000)**	**5.22 (0.000)**	**5.01 (0.000)**
3 systems								
Association	**-1.92 (0.000)**	**-3.62 (0.000)**	**7.28 (0.000)**	**6.06 (0.000)**	**5.69 (0.000)**	**7.18 (0.000)**	**6.22 (0.000)**	**6.80 (0.000)**
Projection	-0.25 (0.444)	**-2.67 (0.000)**	**10.38 (0.000)**	**7.39 (0.000)**	**3.02 (0.000)**	**4.65 (0.000)**	**5.47 (0.000)**	**5.56 (0.000)**
Commissure	**-1.92 (0.000)**	**-2.68 (0.000)**	**7.53 (0.000)**	**3.93 (0.000)**	1.23 (0.018)	0.21 (0.659)	**3.33 (0.000)**	**1.45 (0.003)**
10 subsystems								
Limbic	**-1.06 (0.004)**	**-2.77 (0.000)**	**9.23 (0.000)**	**6.86 (0.000)**	**8.46 (0.000)**	**9.44 (0.000)**	**8.71 (0.000)**	**8.58 (0.000)**
Cortical-Cortical	**-2.46 (0.000)**	**-4.15 (0.000)**	**6.07 (0.000)**	**5.56 (0.000)**	**3.97 (0.000)**	**5.76 (0.000)**	**4.67 (0.000)**	**5.70 (0.000)**
Sensorimotor	0.88 (0.011)	**-1.50 (0.000)**	**4.19 (0.000)**	-0.07 (0.907)	-0.85 (0.026)	0.29 (0.426)	0.83 (0.014)	0.17 (0.608)
FS	**-2.33 (0.000)**	**-5.02 (0.000)**	**17.73 (0.000)**	**16.07 (0.000)**	**9.66 (0.000)**	**11.84 (0.000)**	**12.35 (0.000)**	**13.25 (0.000)**
TR	0.02 (0.963)	**-2.26 (0.000)**	**11.66 (0.000)**	**9.06 (0.000)**	**2.47 (0.000)**	**4.21 (0.000)**	**5.54 (0.000)**	**5.83 (0.000)**
CF_Front	**-7.08 (0.000)**	**-7.75 (0.000)**	**3.04 (0.001)**	-0.08 (0.930)	**3.57 (0.000)**	**3.25 (0.000)**	**3.39 (0.000)**	**2.14 (0.001)**
CF_Par	-1.40 (0.006)	**-1.86 (0.000)**	**9.30 (0.000)**	**5.66 (0.000)**	-0.01 (0.990)	-1.56 (0.021)	**3.09 (0.000)**	0.84 (0.272)
CF_Occ	-1.57 (0.013)	**-2.79 (0.000)**	0.74 (0.530)	1.19 (0.301)	**-2.72 (0.001)**	-0.25 (0.756)	-1.57 (0.028)	0.23 (0.735)
CF_Temp	**3.02 (0.000)**	**1.08 (0.003)**	**13.07 (0.000)**	**5.07 (0.000)**	-0.78 (0.352)	**-3.94 (0.000)**	**3.84 (0.000)**	-0.93 (0.215)
CF_Comm	0.50 (0.371)	**1.49 (0.003)**	**10.46 (0.000)**	**9.64 (0.000)**	0.13 (0.870)	0.77 (0.300)	**3.57 (0.000)**	**3.73 (0.000)**
25 tract groups								
CGB	-0.08 (0.913)	**-2.44 (0.000)**	**5.66 (0.000)**	**5.70 (0.000)**	**3.76 (0.000)**	**5.80 (0.000)**	**4.39 (0.000)**	**5.77 (0.000)**
CGH	-0.82 (0.096)	**-2.47 (0.000)**	**8.06 (0.000)**	**6.43 (0.000)**	**5.19 (0.000)**	**6.87 (0.000)**	**6.15 (0.000)**	**6.72 (0.000)**
FX	**-3.08 (0.000)**	**-3.64 (0.000)**	**25.26 (0.000)**	**7.70 (0.000)**	**16.45 (0.000)**	**5.46 (0.000)**	**19.38 (0.000)**	**6.21 (0.000)**
ST	**2.50 (0.000)**	-0.71 (0.133)	-2.42 (0.062)	**7.63 (0.000)**	**8.92 (0.000)**	**21.67 (0.000)**	**5.14 (0.000)**	**16.99 (0.000)**
UF	**-3.81 (0.000)**	**-4.57 (0.000)**	**9.58 (0.000)**	**6.81 (0.000)**	**7.98 (0.000)**	**7.38 (0.000)**	**8.51 (0.000)**	**7.19 (0.000)**
AF	**-2.31 (0.000)**	**-4.17 (0.000)**	**10.49 (0.000)**	**10.03 (0.000)**	**4.00 (0.000)**	**6.25 (0.000)**	**6.17 (0.000)**	**7.51 (0.000)**
FAT	**-1.92 (0.000)**	**-5.33 (0.000)**	**10.69 (0.000)**	**7.32 (0.000)**	**6.39 (0.000)**	**8.44 (0.000)**	**7.82 (0.000)**	**8.06 (0.000)**
IFOF	**-7.20 (0.000)**	**-7.36 (0.000)**	**2.79 (0.000)**	**3.95 (0.000)**	**8.88 (0.000)**	**9.08 (0.000)**	**6.85 (0.000)**	**7.37 (0.000)**
ILF	**-3.65 (0.000)**	**-3.24 (0.000)**	**10.07 (0.000)**	**9.79 (0.000)**	**6.18 (0.000)**	**5.91 (0.000)**	**7.48 (0.000)**	**7.21 (0.000)**
PF	**1.79 (0.000)**	-1.16 (0.014)	**-3.47 (0.000)**	-0.76 (0.380)	**-6.66 (0.000)**	-0.69 (0.327)	**-5.60 (0.000)**	-0.71 (0.284)
SLF	**-2.14 (0.000)**	**-3.98 (0.000)**	**5.99 (0.000)**	**4.72 (0.000)**	**4.31 (0.000)**	**5.70 (0.000)**	**4.87 (0.000)**	**5.38 (0.000)**
CST	0.99 (0.006)	**-1.58 (0.000)**	**5.19 (0.000)**	0.51 (0.379)	-0.93 (0.019)	0.36 (0.348)	**1.11 (0.001)**	0.40 (0.229)
ML	0.33 (0.432)	-1.07 (0.010)	-0.81 (0.346)	**-2.94 (0.000)**	-0.46 (0.316)	-0.01 (0.978)	-0.57 (0.230)	-0.97 (0.036)
FS_Pfc	**-2.50 (0.000)**	**-4.98 (0.000)**	**18.50 (0.000)**	**16.59 (0.000)**	**10.06 (0.000)**	**11.97 (0.000)**	**12.87 (0.000)**	**13.51 (0.000)**
FS_Mot	**-1.85 (0.000)**	**-5.13 (0.000)**	**15.44 (0.000)**	**14.52 (0.000)**	**8.45 (0.000)**	**11.44 (0.000)**	**10.78 (0.000)**	**12.47 (0.000)**
TR_Pfc	**-2.28 (0.000)**	**-4.86 (0.000)**	**20.84 (0.000)**	**17.49 (0.000)**	**8.80 (0.000)**	**10.47 (0.000)**	**12.81 (0.000)**	**12.81 (0.000)**
TR_Sm	**4.46 (0.000)**	0.88 (0.075)	**15.76 (0.000)**	**10.22 (0.000)**	0.38 (0.495)	**2.44 (0.000)**	**5.50 (0.000)**	**5.03 (0.000)**
TR_Aud	**-1.57 (0.000)**	**-2.47 (0.000)**	**4.62 (0.000)**	1.43 (0.012)	**3.61 (0.000)**	**3.54 (0.000)**	**3.94 (0.000)**	**2.84 (0.000)**
TR_Opt	**-2.69 (0.000)**	**-3.14 (0.000)**	**-7.81 (0.000)**	-2.46 (0.025)	**-7.13 (0.000)**	**-4.07 (0.000)**	**-7.36 (0.000)**	**-3.53 (0.000)**
CF_Pfc	**-8.54 (0.000)**	**-9.15 (0.000)**	0.97 (0.284)	-0.96 (0.271)	**5.00 (0.000)**	**5.08 (0.000)**	**3.66 (0.000)**	**3.07 (0.000)**
CF_Sm	**-3.60 (0.000)**	**-3.88 (0.000)**	**5.58 (0.000)**	**3.89 (0.000)**	**2.85 (0.000)**	**2.21 (0.000)**	**3.76 (0.000)**	**2.77 (0.000)**
CF_Par	-1.40 (0.006)	**-1.86 (0.000)**	**9.30 (0.000)**	**5.66 (0.000)**	-0.01 (0.990)	-1.56 (0.021)	**3.09 (0.000)**	0.84 (0.272)
CF_Occ	-1.57 (0.013)	**-2.79 (0.000)**	0.74 (0.530)	1.19 (0.301)	**-2.72 (0.001)**	-0.25 (0.756)	-1.57 (0.028)	0.23 (0.735)
CF_Temp	**3.02 (0.000)**	1.08 (0.003)	**13.07 (0.000)**	**5.07 (0.000)**	-0.78 (0.352)	**-3.94 (0.000)**	**3.84 (0.000)**	-0.93 (0.215)
CF_Comm	0.50 (0.371)	1.49 (0.003)	**10.46 (0.000)**	**9.64 (0.000)**	0.13 (0.870)	0.77 (0.300)	**3.57 (0.000)**	**3.73 (0.000)**

76 tracts								
L CGB	-1.38 (0.080)	-2.97 (0.000)	3.14 (0.017)	4.26 (0.000)	4.46 (0.000)	5.92 (0.000)	4.02 (0.000)	5.37 (0.000)
R CGB	1.23 (0.137)	-1.90 (0.017)	8.18 (0.000)	7.14 (0.000)	3.05 (0.000)	5.68 (0.000)	4.76 (0.000)	6.16 (0.000)
L CGH	-0.04 (0.954)	-2.27 (0.000)	5.94 (0.000)	1.87 (0.065)	2.23 (0.008)	3.06 (0.000)	3.47 (0.000)	2.66 (0.000)
R CGH	-1.61 (0.003)	-2.68 (0.000)	10.17 (0.000)	10.99 (0.000)	8.15 (0.000)	10.68 (0.000)	8.82 (0.000)	10.78 (0.000)
L FX	-0.22 (0.677)	-2.14 (0.000)	31.03 (0.000)	11.90 (0.000)	10.39 (0.000)	2.17 (0.128)	17.27 (0.000)	5.41 (0.000)
R FX	-5.94 (0.000)	-5.14 (0.000)	19.48 (0.000)	3.51 (0.017)	22.51 (0.000)	8.76 (0.000)	21.50 (0.000)	7.01 (0.000)
L ST	3.75 (0.000)	-0.22 (0.670)	-17.41 (0.000)	2.84 (0.076)	0.07 (0.964)	21.10 (0.000)	-5.76 (0.000)	15.01 (0.000)
R ST	1.25 (0.013)	-1.20 (0.014)	12.58 (0.000)	12.42 (0.000)	17.78 (0.000)	22.25 (0.000)	16.04 (0.000)	18.97 (0.000)
L UF	-3.46 (0.000)	-3.67 (0.000)	10.15 (0.000)	8.05 (0.000)	7.57 (0.000)	6.85 (0.000)	8.43 (0.000)	7.25 (0.000)
R UF	-4.16 (0.000)	-5.48 (0.000)	9.01 (0.000)	5.58 (0.000)	8.39 (0.000)	7.90 (0.000)	8.60 (0.000)	7.13 (0.000)
L AF	-3.34 (0.000)	-5.47 (0.000)	10.00 (0.000)	9.23 (0.000)	4.75 (0.000)	7.19 (0.000)	6.50 (0.000)	7.87 (0.000)
R AF	-1.29 (0.026)	-2.87 (0.000)	10.99 (0.000)	10.82 (0.000)	3.26 (0.000)	5.31 (0.000)	5.84 (0.000)	7.15 (0.000)
L FAT	-4.11 (0.000)	-7.75 (0.000)	13.57 (0.000)	9.03 (0.000)	9.22 (0.000)	11.81 (0.000)	10.67 (0.000)	10.88 (0.000)
R FAT	0.27 (0.629)	-2.91 (0.000)	7.80 (0.000)	5.61 (0.000)	3.56 (0.000)	5.07 (0.000)	4.97 (0.000)	5.25 (0.000)
L IFOF	-8.17 (0.000)	-8.04 (0.000)	0.48 (0.539)	2.55 (0.001)	8.91 (0.000)	9.06 (0.000)	6.10 (0.000)	6.89 (0.000)
R IFOF	-6.22 (0.000)	-6.68 (0.000)	5.10 (0.000)	5.35 (0.000)	8.84 (0.000)	9.11 (0.000)	7.59 (0.000)	7.86 (0.000)
L ILF	-2.00 (0.011)	-2.53 (0.001)	10.70 (0.000)	9.27 (0.000)	4.44 (0.000)	4.93 (0.000)	6.53 (0.000)	6.37 (0.000)
R ILF	-5.30 (0.000)	-3.95 (0.000)	9.45 (0.000)	10.31 (0.000)	7.91 (0.000)	6.90 (0.000)	8.42 (0.000)	8.04 (0.000)
L PF	3.71 (0.000)	-0.80 (0.141)	-4.40 (0.000)	-3.69 (0.000)	-9.70 (0.000)	-3.47 (0.000)	-7.94 (0.000)	-3.55 (0.000)
R PF	-0.13 (0.813)	-1.51 (0.007)	-2.54 (0.013)	2.18 (0.029)	-3.62 (0.000)	2.10 (0.006)	-3.26 (0.000)	2.12 (0.003)
L SLF I	-2.22 (0.000)	-5.74 (0.000)	5.16 (0.000)	2.18 (0.041)	4.77 (0.000)	7.07 (0.000)	4.90 (0.000)	5.44 (0.000)
R SLF I	-5.37 (0.000)	-6.64 (0.000)	4.25 (0.000)	2.44 (0.020)	8.02 (0.000)	8.78 (0.000)	6.76 (0.000)	6.66 (0.000)
L SLF II	-1.63 (0.008)	-2.87 (0.000)	6.85 (0.000)	6.08 (0.000)	3.76 (0.000)	4.80 (0.000)	4.79 (0.000)	5.22 (0.000)
R SLF II	0.27 (0.650)	-1.41 (0.013)	7.02 (0.000)	7.29 (0.000)	1.53 (0.011)	3.84 (0.000)	3.36 (0.000)	4.99 (0.000)
L SLF III	-2.81 (0.000)	-3.76 (0.000)	8.05 (0.000)	8.02 (0.000)	5.92 (0.000)	7.02 (0.000)	6.63 (0.000)	7.35 (0.000)
R SLF III	-1.08 (0.141)	-3.44 (0.000)	4.58 (0.000)	2.29 (0.031)	1.88 (0.006)	2.72 (0.000)	2.78 (0.000)	2.58 (0.000)
L CST_Toe	0.25 (0.605)	-2.42 (0.000)	1.07 (0.208)	-3.82 (0.000)	-1.13 (0.018)	-0.10 (0.828)	-0.38 (0.319)	-1.32 (0.001)
R CST_Toe	2.34 (0.000)	-0.26 (0.559)	4.23 (0.000)	-0.31 (0.674)	-3.66 (0.000)	-2.09 (0.000)	-1.00 (0.022)	-1.46 (0.001)
L CST_Trunk	0.39 (0.463)	-2.82 (0.000)	4.16 (0.000)	-1.28 (0.110)	-0.24 (0.619)	1.54 (0.001)	1.19 (0.001)	0.53 (0.143)
R CST_Trunk	1.48 (0.001)	-0.66 (0.128)	4.30 (0.000)	-1.60 (0.049)	-5.32 (0.000)	-5.31 (0.000)	-2.11 (0.001)	-4.07 (0.000)
L CST_Hand	2.25 (0.000)	-0.54 (0.174)	8.37 (0.000)	3.17 (0.000)	-1.95 (0.000)	-0.28 (0.524)	1.49 (0.000)	0.88 (0.019)
R CST_Hand	3.61 (0.000)	0.60 (0.166)	8.11 (0.000)	2.74 (0.000)	-1.91 (0.000)	-0.25 (0.565)	1.42 (0.000)	0.71 (0.046)
L CST_Mouth	1.36 (0.002)	-1.96 (0.000)	4.36 (0.000)	-0.54 (0.486)	-1.08 (0.029)	1.44 (0.005)	0.67 (0.127)	0.74 (0.109)
R CST_Mouth	1.67 (0.001)	-0.82 (0.075)	5.89 (0.000)	-0.37 (0.661)	-1.55 (0.005)	-0.92 (0.113)	0.94 (0.044)	-0.75 (0.137)
L CST_Geniculate	-1.42 (0.000)	-3.27 (0.000)	5.15 (0.000)	2.61 (0.000)	3.58 (0.000)	4.53 (0.000)	4.11 (0.000)	3.89 (0.000)
R CST_Geniculate	-2.04 (0.000)	-3.69 (0.000)	6.21 (0.000)	4.48 (0.000)	4.01 (0.000)	5.00 (0.000)	4.74 (0.000)	4.85 (0.000)
L ML	-0.83 (0.069)	-2.06 (0.000)	-2.07 (0.030)	-3.15 (0.001)	0.81 (0.106)	1.31 (0.007)	-0.11 (0.837)	-0.14 (0.777)
R ML	1.49 (0.002)	-0.08 (0.868)	0.45 (0.610)	-2.73 (0.001)	-1.73 (0.001)	-1.34 (0.010)	-1.02 (0.040)	-1.80 (0.000)
L FS_OFC	-2.95 (0.000)	-3.48 (0.000)	8.21 (0.000)	8.32 (0.000)	5.72 (0.000)	6.26 (0.000)	6.55 (0.000)	6.94 (0.000)
R FS_OFC	-4.06 (0.000)	-3.61 (0.000)	9.16 (0.000)	8.68 (0.000)	7.29 (0.000)	6.22 (0.000)	7.91 (0.000)	7.04 (0.000)
L FS_VLPFC	-1.22 (0.089)	-5.64 (0.000)	25.36 (0.000)	24.68 (0.000)	14.95 (0.000)	19.26 (0.000)	18.42 (0.000)	21.06 (0.000)
R FS_VLPFC	-0.96 (0.165)	-5.10 (0.000)	24.34 (0.000)	23.20 (0.000)	13.54 (0.000)	17.50 (0.000)	17.14 (0.000)	19.40 (0.000)
L FS_DLPFC	-2.88 (0.000)	-5.51 (0.000)	21.62 (0.000)	18.14 (0.000)	9.82 (0.000)	11.36 (0.000)	13.75 (0.000)	13.62 (0.000)
R FS_DLPFC	-2.91 (0.000)	-6.55 (0.000)	22.29 (0.000)	16.51 (0.000)	9.03 (0.000)	11.20 (0.000)	13.45 (0.000)	12.97 (0.000)
L FS_Mot	-1.70 (0.004)	-5.37 (0.000)	14.82 (0.000)	14.39 (0.000)	7.95 (0.000)	11.75 (0.000)	10.24 (0.000)	12.63 (0.000)
R FS_Mot	-1.99 (0.001)	-4.90 (0.000)	16.07 (0.000)	14.65 (0.000)	8.95 (0.000)	11.14 (0.000)	11.32 (0.000)	12.31 (0.000)
L TR_VLPFC	-3.33 (0.000)	-6.06 (0.000)	20.07 (0.000)	17.99 (0.000)	9.98 (0.000)	12.17 (0.000)	13.34 (0.000)	14.11 (0.000)
R TR_VLPFC	-3.19 (0.000)	-4.35 (0.000)	21.35 (0.000)	20.24 (0.000)	11.24 (0.000)	11.88 (0.000)	14.61 (0.000)	14.67 (0.000)
L TR_DLPFC	-1.44 (0.001)	-4.51 (0.000)	20.60 (0.000)	15.86 (0.000)	6.92 (0.000)	8.81 (0.000)	11.48 (0.000)	11.16 (0.000)
R TR_DLPFC	-1.17 (0.007)	-4.53 (0.000)	21.32 (0.000)	15.86 (0.000)	7.07 (0.000)	9.00 (0.000)	11.82 (0.000)	11.28 (0.000)
L TR_Precentral	3.34 (0.000)	-0.74 (0.215)	15.01 (0.000)	10.03 (0.000)	2.15 (0.000)	4.84 (0.000)	6.44 (0.000)	6.57 (0.000)
R TR_Precentral	4.13 (0.000)	0.12 (0.830)	17.55 (0.000)	11.50 (0.000)	1.88 (0.001)	4.30 (0.000)	7.10 (0.000)	6.70 (0.000)
L TR_Postcentral	5.37 (0.000)	2.55 (0.000)	14.18 (0.000)	8.06 (0.000)	-2.25 (0.001)	-1.43 (0.027)	3.22 (0.000)	1.73 (0.004)
R TR_Postcentral	5.00 (0.000)	1.57 (0.003)	16.28 (0.000)	11.30 (0.000)	-0.26 (0.673)	2.04 (0.001)	5.26 (0.000)	5.13 (0.000)
L TR_Aud	-2.23 (0.000)	-3.01 (0.000)	2.53 (0.000)	0.25 (0.694)	2.58 (0.000)	3.07 (0.000)	2.56 (0.000)	2.13 (0.000)
R TR_Aud	-0.91 (0.033)	-1.92 (0.000)	6.70 (0.000)	2.61 (0.000)	4.64 (0.000)	4.01 (0.000)	5.33 (0.000)	3.54 (0.000)
L TR_Opt	-2.99 (0.000)	-3.33 (0.000)	-8.68 (0.000)	-2.24 (0.069)	-7.90 (0.000)	-4.36 (0.000)	-8.16 (0.000)	-3.65 (0.000)
R TR_Opt	-2.39 (0.000)	-2.95 (0.000)	-6.94 (0.000)	-2.69 (0.026)	-6.37 (0.000)	-3.77 (0.000)	-6.56 (0.000)	-3.41 (0.000)
CF_Genu	-10.61 (0.000)	-10.72 (0.000)	0.41 (0.680)	-0.48 (0.622)	8.19 (0.000)	8.47 (0.000)	5.59 (0.000)	5.49 (0.000)
CF_DLPFC	-10.65 (0.000)	-10.97 (0.000)	7.55 (0.000)	8.32 (0.000)	15.13 (0.000)	15.08 (0.000)	12.61 (0.000)	12.83 (0.000)
CF_VLPFC	-5.29 (0.000)	-7.07 (0.000)	-9.31 (0.000)	-17.07 (0.000)	-13.34 (0.000)	-13.04 (0.000)	-12.00 (0.000)	-14.38 (0.000)
CF_SMA	-7.59 (0.000)	-7.83 (0.000)	5.24 (0.000)	5.40 (0.000)	10.01 (0.000)	9.82 (0.000)	8.42 (0.000)	8.35 (0.000)
CF_Precentral	-1.28 (0.004)	-2.14 (0.000)	11.29 (0.000)	3.45 (0.001)	-2.13 (0.011)	-4.07 (0.000)	2.34 (0.007)	-1.56 (0.050)
CF_Postcentral	-2.63 (0.000)	-3.77 (0.000)	7.97 (0.000)	7.12 (0.000)	4.37 (0.000)	5.11 (0.000)	5.57 (0.000)	5.78 (0.000)
CF_Paracentral	-6.90 (0.000)	-5.74 (0.000)	-2.52 (0.015)	1.10 (0.288)	6.33 (0.000)	5.59 (0.000)	3.38 (0.000)	4.09 (0.000)
CF_SPL	-3.47 (0.000)	-4.13 (0.000)	9.12 (0.000)	8.20 (0.000)	5.45 (0.000)	6.91 (0.000)	6.67 (0.000)	7.34 (0.000)
CF_IPL	1.10 (0.037)	-0.75 (0.134)	22.45 (0.000)	15.12 (0.000)	-0.21 (0.788)	-0.78 (0.310)	7.34 (0.000)	4.52 (0.000)
CF_Precuneus	-1.82 (0.046)	-0.68 (0.464)	-3.65 (0.274)	-6.35 (0.051)	-5.26 (0.000)	-10.82 (0.000)	-4.73 (0.006)	-9.33 (0.000)
CF_Occ	-1.57 (0.013)	-2.79 (0.000)	0.74 (0.530)	1.19 (0.301)	-2.72 (0.001)	-0.25 (0.756)	-1.57 (0.028)	0.23 (0.735)
CF_Sup Temp	3.62 (0.000)	1.95 (0.000)	21.16 (0.000)	12.55 (0.000)	-5.98 (0.000)	-7.21 (0.000)	3.06 (0.000)	-0.62 (0.423)
CF_Mid Temp	2.94 (0.000)	0.19 (0.686)	8.44 (0.000)	8.08 (0.000)	-8.06 (0.000)	-3.70 (0.000)	-2.56 (0.001)	0.23 (0.754)
CF_Temp Pole	4.01 (0.000)	1.73 (0.000)	5.83 (0.000)	-5.33 (0.000)	-3.24 (0.006)	-9.35 (0.000)	-0.22 (0.854)	-8.01 (0.000)
CF_Hippo	4.63 (0.000)	2.60 (0.000)	12.20 (0.000)	-3.57 (0.131)	3.66 (0.087)	-6.90 (0.000)	6.50 (0.002)	-5.79 (0.004)
CF_Amyg	-0.08 (0.875)	-1.07 (0.023)	17.75 (0.000)	13.63 (0.000)	9.73 (0.000)	7.47 (0.000)	12.40 (0.000)	9.53 (0.000)
CF_AC	-2.17 (0.041)	1.93 (0.048)	-4.93 (0.017)	-1.31 (0.469)	-3.24 (0.003)	-2.31 (0.019)	-3.81 (0.002)	-1.98 (0.055)
CF_PC	3.17 (0.000)	1.05 (0.004)	25.86 (0.000)	20.60 (0.000)	3.50 (0.000)	3.85 (0.000)	10.95 (0.000)	9.44 (0.000)

3.3. Spatial patterns of age-related difference in GFA, AD, RD and MD

Fig. 2 shows the 76 tracts color-coded with β_1 of GFA, with men and women rendered separately. In general, GFA decreased with age in both men and women, as presented by the predominantly blue hue on the tracts. However, some tracts presented a higher GFA with age, deviating from the global trend. In the association fibers, most tracts exhibited lower GFA with age; only the stria terminalis (ST) and PF exhibited higher GFA with age. The commissure fibers exhibited a gradient difference in GFA from the anterior brain (most prominent difference in the prefrontal lobe) to the posterior brain (least prominent difference in the parietal and occipital lobes). By contrast, the commissure fibers connecting the temporal lobe exhibited higher GFA with age. In the projection fibers, the frontostriatal tracts and thalamic radiations connecting the prefrontal lobe and visual cortex exhibited lower GFA with age, whereas the CST and thalamic radiations connecting the somatosensory cortex showed higher GFA with age. Both men and women demonstrated a similar pattern of GFA difference with age, but women tended to have a more negative difference (negative β_1) and less positive difference (positive β_1) than did men.

Fig. 2. The 76 tracts color-coded for the age-related differences in GFA. Red color indicates tracts with significant positive differences with age, blue color indicates tracts with significant negative differences with age, and gray color indicates tracts without significant age-related differences. Association (upper row), projection (middle row), and commissure (lower row) fibers are rendered separately for male (left) and female (right) participants. To visualize the age-related differences, the magnitude of β_1 value was rescaled

by 10^4.

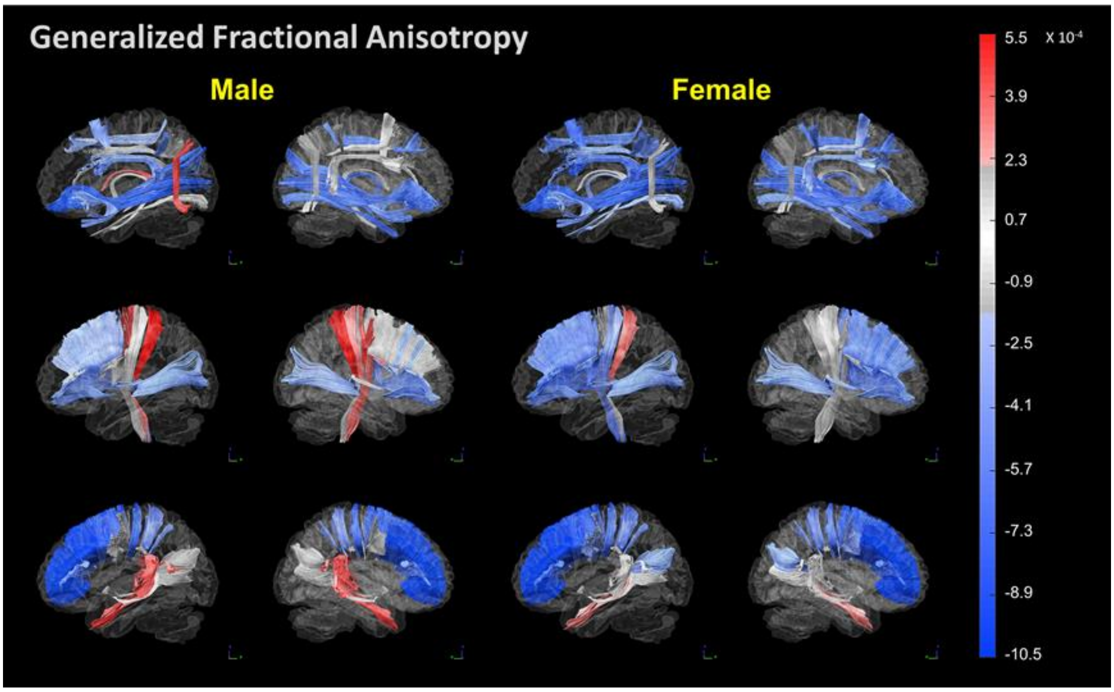

Figure 3 shows the magnitude of β_1 values of GFA in the 76-tract level and the 25 tract-group level placed side-by-side, with men and women displayed separately. Although the 76-tract level showed more details in the age difference across different tracts, the spatial pattern remained consistent in the 25-tract-group level. Particularly, the tracts of atypical age-related difference (bars labeled in red) observed in the 76-tract level were mostly present in the 25-tract-group level. The only exceptions were the corticospinal tracts in men, and the callosal fibers to the temporal lobe in women. There are mild significant differences in the 76-tract level (i.e., right CST_toe, CST_hand, CST_mouth, and left CST_hand in male corticospinal tracts, and CF_Sup Temp, CF_Temp Pole, CF_Hippo in female callosal fibers to the temporal lobe), and they became non-significant in the 25-tract-group level (i.e. male CST and female CF_Temp).

Both levels showed that male participants had more tracts with significant positive β_1 values, whereas female participants had more tracts with significant negative β_1 values. Moreover, male participants presented significant positive β_1 values with magnitudes larger than those in female participants. By contrast, female participants had significant negative β_1 values with magnitudes generally larger than those in male participants. Of the 76 tracts, the male and female participants had 31 (41%) and 51 (67%) tracts with significant negative β_1 values, respectively. The results indicate that women had more prominent negative differences in tract properties than did men ($\chi^2 = 10.59$, $p = 0.001$).

Fig. 3. The bar charts of the magnitude of the age-related differences (β_1) in GFA in the 76-tract level (left) and the 25 tract group level (right). Men and women are displayed in (A) and (B), respectively. Red color indicates significant positive β_1 values, blue color indicates significant negative β_1 values, and gray color indicates β_1 values without statistical significance. To visualize the age-related differences, the magnitude of β_1 values was rescaled by 10^4.

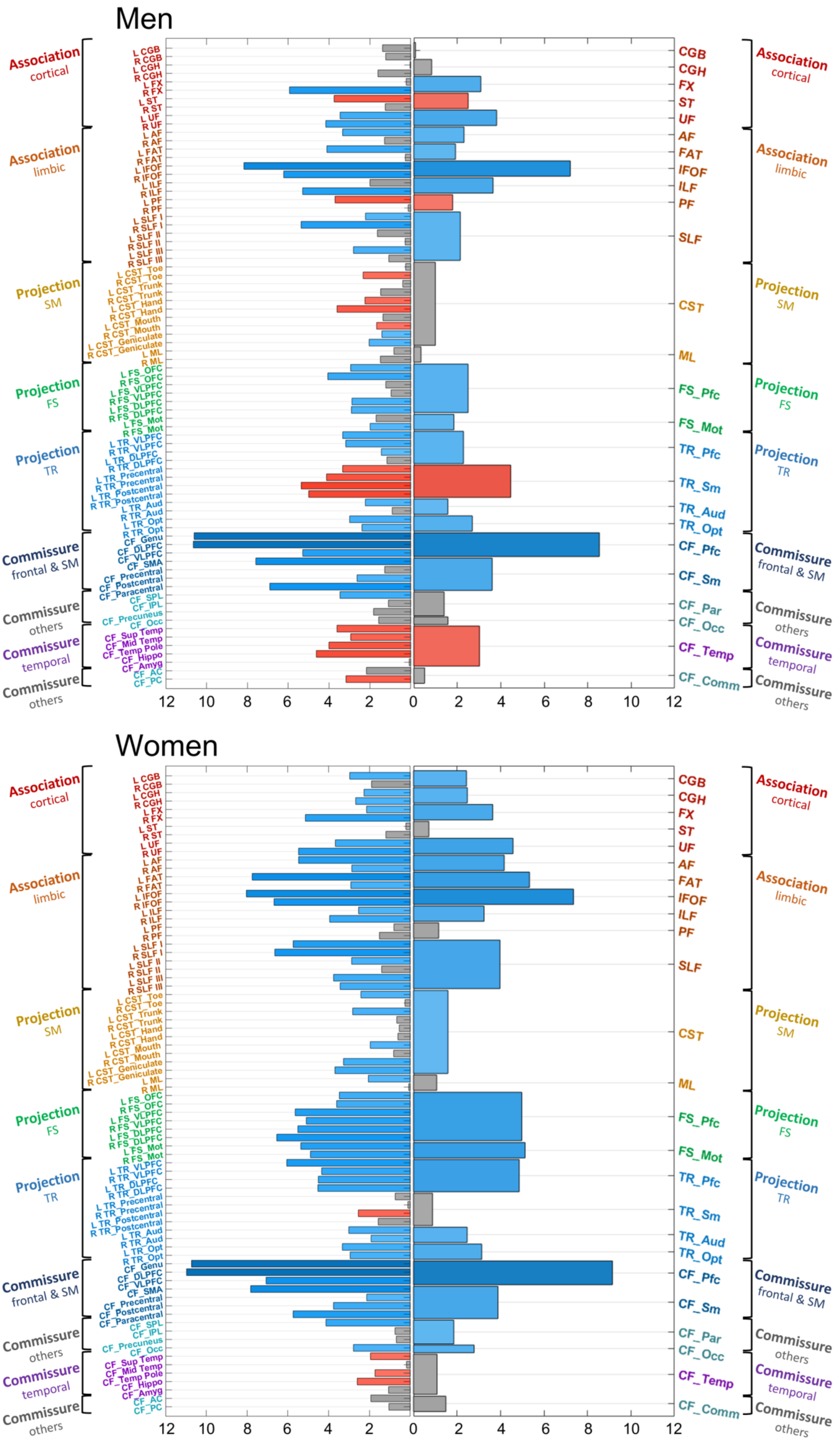
Men
Women
Association cortical
Association limbic
Projection SM
Projection FS
Projection TR
Commissure frontal & SM
Commissure others
Commissure temporal
Commissure others
L CGB
R CGB
L CGH
R CGH
L FX
R FX
L ST
R ST
L UF
R UF
L AF
R AF
L FAT
R FAT
L IFOF
R IFOF
L ILF
R ILF
L PF
R PF
L SLF I
R SLF I
L SLF II
R SLF II
L SLF III
R SLF III
L CST_Toe
R CST_Toe
L CST_Trunk
R CST_Trunk
L CST_Hand
R CST_Hand
L CST_Mouth
R CST_Mouth
L CST_Geniculate
R CST_Geniculate
L ML
R ML
L FS_OFC
R FS_OFC
L FS_VLPFC
R FS_VLPFC
L FS_DLPFC
R FS_DLPFC
L FS_Mot
R FS_Mot
L TR_VLPFC
R TR_VLPFC
L TR_DLPFC
R TR_DLPFC
L TR_Precentral
R TR_Precentral
L TR_Postcentral
R TR_Postcentral
L TR_Aud
R TR_Aud
L TR_Opt
R TR_Opt
CF_Genu
CF_DLPFC
CF_VLPFC
CF_SMA
CF_Precentral
CF_Postcentral
CF_Paracentral
CF_SPL
CF_IPL
CF_Precuneus
CF_Occ
CF_Sup Temp
CF_Mid Temp
CF_Temp Pole
CF_Hippo
CF_Amyg
CF_AC
CF_PC
CGB
CGH
FX
ST
UF
AF
FAT
IFOF
ILF
PF
SLF
CST
ML
FS_Pfc
FS_Mot
TR_Pfc
TR_Sm
TR_Aud
TR_Opt
CF_Pfc
CF_Sm
CF_Par
CF_Occ
CF_Temp
CF_Comm
12 10 8 6 4 2 0
0 2 4 6 8 10 12

1

Supplementary Fig. 5A presented the 76 tracts color-coded with β_1 values of AD, and Supplementary Fig. 5B shows the bar charts in the 76-tract level and the 25 tract-group level, with men and women displayed separately. A predominant trend of higher AD with age was observed, with the projection fibers connecting the frontal lobe exhibiting the most prominent positive difference. A small number of tracts showed significantly lower AD with age; these tracts were distributed in the association fibers (left ST, left PF), projection fibers (left CST_Toe, left medial lemniscus (ML), bilateral TR_Opt), and commissure fibers (CF_VLPFC and CF_Temp pole).

Supplementary Fig. 5C illustrates the 76 tracts color-coded with β_1 values of RD, and Supplementary Fig. 5D shows the bar charts in the 76-tract level and the 25 tract-group level. A predominant trend of higher RD with age was observed, and it involved most of the association fibers and the projection and commissure fibers connecting the frontal lobe. A small number of tracts showed significantly lower RD with age and these were most prevalent among the callosal fibers (CF_VLPFC, CF_Precentral, CF_Precuneus, CF_Occ, and all callosal fibers connecting the temporal lobe), followed by the projection fibers (CST_Hand, CST_Trunk and CST_Toe, and bilateral TR_Opt), and the association fibers (bilateral PF).

Supplementary Fig. 5E presents the 76 tracts color-coded with β_1 values of MD, and Supplementary Fig. 5F shows the bar charts in the 76-tract level and the 25 tract-group level. A predominant trend of higher MD with age was observed, and the pattern was similar to that of RD; the tracts involved most of the association, projection and commissure fibers connecting the frontal lobe. However, tracts that presented significant lower MD with age had a pattern similar to that of AD and mostly involved the association (left

ST, bilateral PF), projection (left CST_Toe, right CST_Trunk, right ML, bilateral TR_Opt), and commissure fibers (CF_VLPFC, CF_precuneus, and CF_Temp pole).

3.4. Normative values of WM tract properties in the UK Biobank cohort

The mean values of GFA, AD, RD, and MD of all WM tracts for each year were analyzed; the values are listed in Supplementary Table 3, and a plot of these values is presented in Supplementary Fig. 6. A normality test was performed for each tract for each year and sex. In a total of 18,240 tests (i.e., 4 indices ×76 tracts × 30 years × 2 sexes = 18,240), only 30 tests failed the test. Therefore, the means and standard deviations of diffusion indices (including GFA, AD, RD, and MD) were determined for each of the 76 tracts and at each year, with the values in men and women presented separately. By using the β_1 values and mean diffusion indices of the population aged 47 years, the total relative difference across 30 years was calculated for each index at each tract and for each sex. We observed that the difference in tract properties from ages of 47 to 76 years was not very large. The total relative difference across 30 years was at most 13% with respect to the initial tract properties at the age of 47 years. In men, the CF_DLPFC had the greatest negative difference in GFA, and the total relative difference over 30 years was −6%. Moreover, the largest positive differences in AD, RD, and MD were found in the PC (CF_PC), right FX and right FX, respectively, with the total relative difference of 8%, 13%, and 9%, respectively. In women, the CF_DLPFC exhibited the greatest negative difference in GFA, and the total relative difference over 30 years was −6%. Moreover, the largest positive differences in AD, RD, and MD were found in left FS_VLPFC, right ST, and left FS_VLPF, with the total relative difference of 8%, 13%, and 10%, respectively.

4. Discussion

4.1. Summary

This cross-sectional study analyzed the largest cohort of neurologically healthy participants in the world and provided a detailed description of age-related differences in dMRI-derived tract properties across mid to late adulthood. The study results are exceptionally valuable because all MRI data were acquired using the same MRI scanner and analyzed using the same analysis software, thus avoiding the variability due to the use of different scanners or analysis techniques. By using a large sample size and stringent data acquisition and analysis procedures, we observed significant differences in dMRI-derived tract properties in normal aging and their corresponding spatial distributions. A dominant pattern of age-related difference, with lower /insignificant GFA and higher AD, RD, and MD with age, was seen in 59% of the tracts (45 of 76 tracts). This pattern involved most of the association fibers plus the projection and callosal fibers connecting the prefrontal cortices. In addition to the dominant pattern, three atypical patterns were observed in 21% of the tracts (16 of 76 tracts). These atypical patterns might represent milder degrees of age-related differences in tract properties, and mainly involved the projection fibers and callosal fibers connecting the sensorimotor, occipital and temporal cortices.

4.2. Axonal fibers in brain aging

Neurobiological studies have shown that axonal fibers deteriorate more profoundly than neurons during normal aging (Peters et al., 1998). Pakkenberg and Gundersen (1997) reported up to 28% reduction in WM volume, but approximately 10% reduction in cortical neuron number in individuals aged 20–90 years. Multiple studies have also reported that aging effects on axonal fibers are heterogeneous (Aboitiz et al., 1992; Liewald et al., 2014; Tomasi and Volkow, 2012). Thin fibers are more vulnerable to aging effects than are thick fibers, and fibers connecting the prefrontal lobe exhibit more profound aging effects than those connecting the posterior brain (Bartzokis, George, 2004). The heterogeneous aging effects on axonal fibers reflect different vulnerabilities of axonal fibers owing to varied age-related alterations of perfusion, oligodendrocytes and other glial cells (Liu, Huan et al., 2017).

4.3. A dominant pattern of age-related differences in tract properties

This study found a dominant pattern of age-related differences in tract properties (i.e., higher AD, RD, and MD and lower /insignificant GFA with age; Fig. 3 and Table 2). We found that the tracts with this dominant pattern involved most of the association fibers and the prefrontal part of the commissure fibers and projection fibers. Neurobiological studies have reported the presence of abundant thin fibers in the association fibers (Liewald et al., 2014), prefrontal commissure fibers (Aboitiz et al., 1992), and prefrontal projection fibers (Tomasi and Volkow, 2012). Thin fibers have thinner myelin sheaths, mature later in life, and are more vulnerable to aging effect than thick fibers (Liu, H. et al., 2017). The similarity of the spatial distribution reported in this study and that reported in neurobiological studies implies that the dominant pattern of diffusion difference might be related to aging effect of WM microstructures.

Despite differing methodologies, some of the longitudinal dMRI studies observed age-related changes consistent with our findings. Bender et al. found that the association fibers exhibited the most pronounced declines over time (Bender et al., 2016). Their findings support our cross-sectional findings that the dominant pattern of age-related difference mainly involved the association fibers. Sexton et al. observed that the annual change in diffusion indices presented a lobe-specific pattern (Sexton et al., 2014); the decline was most rapid in the frontal lobe, followed by parietal, occipital lobes, and the least in the temporal lobe. This lobe-specific pattern was also observed in our age-related differences in callosal fibers. The spatial patterns reported above lend support to the myelodegeneration hypothesis (Bartzokis, G., 2004; Davis et al., 2009).

Diffusion index profiles only capture some tract properties. Indices derived from other quantitative MRI measurements such as longitudinal relaxivity R1 or magnetisation transfer ratio may represent different WM aging processes (Seiler et al., 2014; Yeatman et al., 2014). Interpretation of underlying microstructural variations merely based on diffusion indices may be oversimplified (Jones et al., 2013). Nevertheless, the present study provides a brain-wide view of tract property differences, which can only be obtained by meta-analysis of previous DTI studies that have found selective age-related differences in the association fibers (Hugenschmidt et al., 2008; Stadlbauer et al., 2008), prefrontal projection fibers (Jang, S. H. and Seo, J. P., 2015), and prefrontal commissure fibers (Sullivan and Pfefferbaum, 2006; Yoon et al., 2008).

Previous DTI studies have reported a dominant pattern of age difference with lower FA, higher RD, and varied AD with age (Bennett et al., 2010; Burzynska et al., 2010). The dominant pattern in our study presented lower GFA, higher RD, and higher AD with age. The inconsistency in AD difference may be caused by differences in age groups. Both the abovementioned DTI studies compared a group of young adults in the age range of 18–32 years with a group of older adults in the age range of 60–72 years (Bennett et al., 2010; Burzynska et al., 2010). By contrast, the age of our participants ranged from 47 to 76 years. Diffusion indices are known to vary nonlinearly across a lifespan. Diffusion anisotropy parameters such as GFA increases from childhood to early adulthood, peaks in the middle age, and decreases afterward (Kochunov et al., 2012), whereas AD, RD, and MD decrease from childhood, reach the minimum in midlife, and increase in later life. The difference in AD between young adults and older adults recruited in previous DTI studies may be smaller than the difference among adults aged 47–76 years in our study, resulting in varied differences in AD.

4.4. Atypical patterns of age-related differences in tract properties

In addition to the dominant pattern, we found three atypical patterns of age-related differences (Table 2). The first pattern presented higher AD, varied RD, higher MD, and higher GFA with age; the second pattern exhibited higher AD, lower RD, higher GFA, and varied MD; and the third showed lower AD, RD, and MD and varied GFA. The first and second patterns shared a pattern of diffusion index variations, namely higher GFA and AD with age. The two patterns also shared a spatial distribution. The tracts included the projection fibers connecting the sensorimotor area (CST_Toe, CST_Hand, and thalamic radiations connecting the precentral and postcentral cortices) and the commissural fibers connecting the temporal and occipital lobes (CF_Sup temp, CF_Mid temp, CF_Temp pole, CF_Hippo, and CF_PC). Our findings are consistent with previous DTI studies that showed relatively spared fibers connecting the sensorimotor cortex (Jang, Sung Ho and Seo, Jeong Pyo, 2015) and temporal and occipital areas (Sullivan et al., 2006;

Yoon et al., 2008). Therefore, these two patterns of diffusion variations may imply a relatively mild form of aging effect.

The third pattern of age difference exhibited lower AD, RD, and MD with age. Except CF_VLPFC, the tracts in the third pattern involved the visual cortex (left PF and bilateral TR_Opt). Like sensorimotor tracts, the tracts to the visual areas have abundant thick fibers known to be resistant to the effects of aging (Bartzokis, G., 2004). Therefore, the third pattern might imply another form of mild aging effect. Although CF_VLPFC belongs to the callosal fibers connecting the prefrontal lobe, it exhibited a completely opposite age difference pattern compared with other callosal fibers of the prefrontal lobe. Further research is required to investigate the mechanism of the opposite age difference of this tract.

4.5. Age-related tract differences in women

This study found that female participants presented more tracts with significant negative differences in tract properties (i.e., GFA) than male participants. A similar sex difference in age-related differences of tract properties has been reported previously and is considered to be partially related to menopausal effects (Berent-Spillson et al., 2012; Ha et al., 2007; Mosconi et al., 2017; Mosconi et al., 2018; Peper et al., 2011; Ycaza Herrera and Mather, 2015). Because participant age in this study ranged from 47 to 76 years, the women were a mix of premenopausal, perimenopausal,and postmenopausal. Estrogen is known to have potent neuroprotective effects, and reduced estrogen concentration in female-specific endocrine transitions has been found to be associated with alterations of WM in aging, enhanced Alzheimer's disease–related pathologies in the brain, cognitive decline, and neurodegenerative disease in elderly women (Berent-

Spillson et al., 2012; Ha et al., 2007; Mosconi et al., 2017; Mosconi et al., 2018; Peper et al., 2011; Ycaza Herrera and Mather, 2015). Although some participants may have received hormone therapy, the effect is inconsistent and the number of medicated women may be too low to balance the overall reduction of estrogen in the population. In addition to the menopausal effects, factors such as education, occupation, lifestyle, and cardiovascular risks may modulate WM properties (Tian et al., 2015; Williamson et al., 2018). Further research is required to investigate the causes of aggravated deficits of dMRI-derived tract properties in women after middle age.

4.6. Magnitude of differences in tract properties with age

A contribution of this study is that it provides comprehensive data of age-related differences in tract properties from 47 to 76 years of age (Supplementary Table 3 and Supplementary Fig. 6). These normative data allowed us to estimate the relative amount of difference over the span of 30 years in late adulthood. Relative to the initial index values at 47 years of age, the relative amount of difference was not larger than 13% over 30 years or 0.43% per year. The magnitude of the difference is comparable to the fitted results on a lifespan cohort interpreted in the same age range of (Lebel et al., 2012) and the longitudinal results on a cohort scanned at 73 and 76 years of age (Ritchie et al., 2017). Amlien et al. (Amlien et al., 2013) conducted a longitudinal study on patients with mild cognitive impairment and found a greater rate of decline in WM properties in these patients than in healthy people. By using the normative data for tract-specific age differences in normal aging, we can detect advanced aging effects on specific tracts in pathological brain aging. For instance, a longitudinal study on a group of participants who were mutation carriers of early-onset autosomal-dominant Alzheimer's disease showed a change of 0.27% per year in the IFOF and genu of the corpus callosum (Araque Caballero et al., 2018), exceeding the estimated age-related differences of 0.13% and 0.08% in our healthy population, respectively.

4.7. Limitations

The study has limitations that may necessitate cautious interpretation of the results. First, the study used a cross-sectional design. The β_1 derived from these values is deemed different from the values of the slope obtained from longitudinal studies that have followed up the same cohort over time (Pfefferbaum and Sullivan, 2015). Hypothetically, the longitudinal design is superior to the cross-sectional design in describing age-related change of diffusion indices because additional information of interval change of each individual is provided. However, the measured interval change may not purely come from the brain change, it may also come from the system change during the observation interval. Constant system calibration is needed to control this confounding factor in both longitudinal and cross-sectional studies. Second, the age range of the participants was 47–76 years and the total amount of difference over this age range was quite small (only 13% at most). The age differences in tract properties may accelerate with advancing age, as observed by a longitudinal study on 5286 people in the Rotterdam Study (Vinke et al., 2018). In addition, we found some tracts showing little age difference in this age range. Investigating the trajectories of these tracts since young adulthood is noteworthy. Such questions can be answered by the Rhineland study, an ongoing longitudinal study, which plans to recruit 30,000 community-based people aged 30 years or over at baseline (Breteler and Wolf, 2014). Third, the study participants came from a community-dwelling population who had no history of neurological and psychiatric disease, substance abuse, and malignancy and had an IQ within normal range. However, the participants might have varied degrees of WM hyperintensity lesions which might confound the diffusion index values and change the age-difference patterns. Schelten's scale or a reliable quantitative tool for lesion segmentation is needed to regress out this confounding factor. Fourth, although we have provided evidence to address the concerns of registration accuracy, we still acknowledge that the error incurred from individual variation of the gyral folding is inevitable. According to tract anatomy, the portion of the tract sitting in such error-prone regions is less than 30% (Zhang et al., 2018). If there is only 50% overlap between template tracts and an individual's 'real' tracts, the error is estimated to be less than 15%. Finally, this study used MAP-MRI to reconstruct diffusion PDF, and from which quantified diffusion indices. We then employed TBAA to sample diffusion index values on 76 white matter fiber tracts. Comparing our results with others' using different diffusion reconstruction or sampling methods would be very challenging because it is unclear whether the disparity of the results is due to methodological difference or other factors related to study populations or imaging techniques. Unification of core imaging protocols and process pipelines would facilitate the comparison across different studies.

5. Conclusions

By analyzing dMRI data from 7167 UK Biobank participants, this paper has provided a detailed description of heterogeneity of age-related differences in tract properties in a healthy community-dwelling population aged 47 to 76 years. Profiles of age-related differences in diffusion indices and the corresponding spatial patterns as revealed at 5 levels of tract grouping characterize a specific heterogeneous aging effect. The dominant patterns of age-related differences in tract properties were concentrated in the frontal lobe, corresponding to a relatively profound aging effect. By contrast, the atypical patterns of age-related differences were distributed in the posterior brain and temporal lobe, corresponding to a milder form of aging. The tract-wise relative differences in dMRI indices generally support the myelodegeneration hypothesis and can serve as a reference of normal aging effects.

Acknowledgments

This research was approved by the UK Biobank (application number: 24089) and was supported by the Roland Sutton Academic Trust (grant number: 0039/R/16) and Taiwan National Health Research Institute (NHRI-EX109-10928NI). We acknowledge the valuable contributions of members of the UK Biobank Imaging Working Group and the UK Biobank coordinating center. The UK Biobank (including the imaging enhancement) was supported by the UK Medical Research Council and the Wellcome Trust. We are grateful for the provision of simultaneous multislice (multiband) pulse sequence and reconstruction algorithms by the Center for Magnetic Resonance Research, University of Minnesota. Finally, we are extremely grateful to all UK Biobank study participants, who have generously donated their time to make this resource possible. This manuscript was edited by Wallace Academic Editing.

References

Aboitiz, F., Scheibel, A.B., Fisher, R.S., Zaidel, E., 1992. Fiber composition of the human corpus callosum. Brain research 598, 143-153.

Ackman, J.B., Burbridge, T.J., Crair, M.C., 2012. Retinal waves coordinate patterned activity throughout the developing visual system. Nature 490(7419), 219-225.

Alexander, A.L., Hurley, S.A., Samsonov, A.A., Adluru, N., Hosseinbor, A.P., Mossahebi, P., Tromp do, P.M., Zakszewski, E., Field, A.S., 2011. Characterization of cerebral white matter properties using quantitative magnetic resonance imaging stains. Brain Connect 1(6), 423-446.

Amlien, I., Fjell, A.M., Walhovd, K.B., Selnes, P., Stenset, V., Grambaite, R., Bjornerud, A., Due-Tonnessen, P., Skinningsrud, A., Gjerstad, L., Reinvang, I., Fladby, T., 2013. Mild Cognitive Impairment: Cerebrospinal Fluid Tau Biomarker Pathologic Levels and Longitudinal Changes in White Matter Integrity. Radiology 266, 295-303.

Andersson, J.L., Skare, S., Ashburner, J., 2003. How to correct susceptibility distortions in spin-echo echo-planar images: application to diffusion tensor imaging. Neuroimage 20(2), 870-888.

Andersson, J.L., Sotiropoulos, S.N., 2015. Non-parametric representation and prediction of single- and multi-shell diffusion-weighted MRI data using Gaussian processes. Neuroimage 122, 166-176.

Andersson, J.L.R., Sotiropoulos, S.N., 2016. An integrated approach to correction for off-resonance effects and subject movement in diffusion MR imaging. Neuroimage 125, 1063-1078.

Antonenko, D., Floel, A., 2014. Healthy aging by staying selectively connected: a mini-review. Gerontology 60(1), 3-9.

Araque Caballero, M.A., Suarez-Calvet, M., Duering, M., Franzmeier, N., Benzinger, T., Fagan, A.M., Bateman, R.J., Jack, C.R., Levin, J., Dichgans, M., Jucker, M., Karch, C., Masters, C.L., Morris, J.C., Weiner, M., Rossor, M., Fox, N.C., Lee, J.H., Salloway, S., Danek, A., Goate, A., Yakushev, I., Hassenstab, J., Schofield, P.R., Haass, C., Ewers, M., 2018. White matter diffusion alterations precede symptom onset in autosomal dominant Alzheimer's disease. Brain : a journal of neurology 141(10), 3065-3080.

Ashburner, J., Friston, K.J., 2011. Diffeomorphic registration using geodesic shooting and Gauss-Newton optimisation. Neuroimage 55(3), 954-967.

Bartzokis, G., 2004. Age-related myelin breakdown: a developmental model of cognitive decline and Alzheimer's disease. Neurobiology and Aging 25, 5-18.

Bartzokis, G., 2004. Age-related myelin breakdown: a developmental model of cognitive decline and Alzheimer’s disease. Neurobiology of aging 25(1), 5-18.

Basser, P.J., Mattiello, J., LeBihan, D., 1994. MR Diffusion Tensor Spectroscopy and Imaging. Biophysical Journal 66, 259-267.

Beaulieu, C., 2002. The basis of anisotropic water diffusion in the nervous system - a technical review. NMR Biomed 15(7-8), 435-455.

Bender, A.R., Volkle, M.C., Raz, N., 2016. Differential aging of cerebral white matter in middle-aged and older adults: A seven-year follow-up. Neuroimage 125, 74-83.

Bennett, I.J., Madden, D.J., 2014. Disconnected aging: cerebral white matter integrity and age-related

differences in cognition. Neuroscience 276, 187-205.
Bennett, I.J., Madden, D.J., Vaidya, C.J., Howard, D.V., Howard Jr, J.H., 2010. Age-related differences in multiple measures of white matter integrity: A diffusion tensor imaging study of healthy aging. Human brain mapping 31(3), 378-390.
Berent-Spillson, A., Persad, C.C., Love, T., Sowers, M., Randolph, J.F., Zubieta, J.K., Smith, Y.R., 2012. Hormonal environment affects cognition independent of age during the menopause transition. J Clin Endocrinol Metab 97(9), E1686-1694.
Breteler, M.M.B., Wolf, H., 2014. P2-135: The Rhineland Study: A Novel Platform for Epidemiologic Research into Alzheimer Disease and Related Disorders. Alzheimer's & Dementia 10, P520-P520.
Burzynska, A.Z., Preuschhof, C., Bäckman, L., Nyberg, L., Li, S.-C., Lindenberger, U., Heekeren, H.R., 2010. Age-related differences in white matter microstructure: region-specific patterns of diffusivity. Neuroimage 49(3), 2104-2112.
Cao, Y., Miller, M.I., Mori, S., Winslow, R.L., Younes, L., 2006. Diffeomorphic Matching of Diffusion Tensor Images. Proc IEEE Comput Soc Conf Comput Vis Pattern Recognit 2006, 67.
Chen-Plotkin, A.S., 2014. Unbiased approaches to biomarker discovery in neurodegenerative diseases. Neuron 84(3), 594-607.
Chen, Y.J., Liu, C.M., Hsu, Y.C., Lo, Y.C., Hwang, T.J., Hwu, H.G., Lin, Y.T., Tseng, W.I., 2018. Individualized prediction of schizophrenia based on the whole-brain pattern of altered white matter tract integrity. Human brain mapping 39(1), 575-587.
Chen, Y.J., Lo, Y.C., Hsu, Y.C., Fan, C.C., Hwang, T.J., Liu, C.M., Chien, Y.L., Hsieh, M.H., Liu, C.C., Hwu, H.G., Tseng, W.Y., 2015. Automatic whole brain tract-based analysis using predefined tracts in a diffusion spectrum imaging template and an accurate registration strategy. Human brain mapping 36(9), 3441-3458.
Chien, Y.L., Chen, Y.J., Hsu, Y.C., Tseng, W.I., Gau, S.S., 2017. Altered white-matter integrity in unaffected siblings of probands with autism spectrum disorders. Human brain mapping 38(12), 6053-6067.
Cox, S.R., Ritchie, S.J., Tucker-Drob, E.M., Liewald, D.C., Hagenaars, S.P., Davies, G., Wardlaw, J.M., Gale, C.R., Bastin, M.E., Deary, I.J., 2016. Ageing and brain white matter structure in 3,513 UK Biobank participants. Nature communications 7, 13629.
Davis, S.W., Dennis, N.A., Buchler, N.G., White, L.E., Madden, D.J., Cabeza, R., 2009. Assessing the effects of age on long white matter tracts using diffusion tensor tractography. NeuroImage 46(2), 530-541.
Fjell, A.M., McEvoy, L., Holland, D., Dale, A.M., Walhovd, K.B., Initiative, A.s.D.N., 2014. What is normal in normal aging? Effects of aging, amyloid and Alzheimer's disease on the cerebral cortex and the hippocampus. Progress in neurobiology 117, 20-40.
Gold, B.T., Keller, J.N., 2012. Imaging Brain Aging and Neurodegenerative Disease., Biochimica et Biophysica Acta(BBA)- Molecular Basis of Disease. pp. 315-492.
Ha, D.M., Xu, J., Janowsky, J.S., 2007. Preliminary evidence that long-term estrogen use reduces white matter loss in aging. Neurobiology of aging 28(12), 1936-1940.
Hagmann, P., Cammoun, L., Gigandet, X., Meuli, R., Honey, C.J., Wedeen, V.J., Sporns, O., 2008. Mapping the structural core of human cerebral cortex. PLoS Biol 6(7), e159.

Hsu, Y.C., Lo, Y.C., Chen, Y.J., Wedeen, V.J., Isaac Tseng, W.Y., 2015. NTU-DSI-122: A diffusion spectrum imaging template with high anatomical matching to the ICBM-152 space. Human brain mapping 36(9), 3528-3541.

Huang, J.Y., Liu, C.M., Hwang, T.J., Chen, Y.J., Hsu, Y.C., Hwu, H.G., Lin, Y.T., Hsieh, M.H., Liu, C.C., Chien, Y.L., Tseng, W.I., 2018. Shared and distinct alterations of white matter tracts in remitted and nonremitted patients with schizophrenia. Human brain mapping 39(5), 2007-2019.

Hugenschmidt, C.E., Peiffer, A.M., Kraft, R.A., Casanova, R., Deibler, A.R., Burdette, J.H., Maldjian, J.A., Laurienti, P.J., 2008. Relating imaging indices of white matter integrity and volume in healthy older adults. Cerebral cortex 18(2), 433-442.

Jang, S.H., Seo, J.P., 2015. Aging of corticospinal tract fibers according to the cerebral origin in the human brain: a diffusion tensor imaging study. Neuroscience letters 585, 77-81.

Jang, S.H., Seo, J.P., 2015. Aging of corticospinal tract fibers according to the cerebral origin in the human brain: a diffusion tensor imaging study. Neuroscience letters 585, 77-81.

Jones, D.K., Christiansen, K.F., Chapman, R.J., Aggleton, J.P., 2013. Distinct subdivisions of the cingulum bundle revealed by diffusion MRI fibre tracking: implications for neuropsychological investigations. Neuropsychologia 51(1), 67-78.

Koay, C.G., Chang, L.C., Carew, J.D., Pierpaoli, C., Basser, P.J., 2006. A unifying theoretical and algorithmic framework for least squares methods of estimation in diffusion tensor imaging. J Magn Reson 182(1), 115-125.

Kochunov, P., Williamson, D., Lancaster, J., Fox, P., Cornell, J., Blangero, J., Glahn, D., 2012. Fractional anisotropy of water diffusion in cerebral white matter across the lifespan. Neurobiology of aging 33(1), 9-20.

Lebel, C., Gee, M., Camicioli, R., Wieler, M., Martin, W., Beaulieu, C., 2012. Diffusion tensor imaging of white matter tract evolution over the lifespan. Neuroimage 60(1), 340-352.

Liewald, D., Miller, R., Logothetis, N., Wagner, H.J., Schuz, A., 2014. Distribution of axon diameters in cortical white matter: an electron-microscopic study on three human brains and a macaque. Biological cybernetics 108(5), 541-557.

Liu, H., Yang, Y., Xia, Y., Zhu, W., Leak, R.K., Wei, Z., Wang, J., Hu, X., 2017. Aging of cerebral white matter. Ageing research reviews 34, 64-76.

Liu, H., Yang, Y., Xia, Y., Zhu, W., Leak, R.K., Wei, Z., Wang, J., Hu, X., 2017. Aging of cerebral white matter. Ageing research reviews 34, 64-76.

Lo, Y.C., Chen, Y.J., Hsu, Y.C., Chien, Y.L., Gau, S.S., Tseng, W.I., 2019. Altered frontal aslant tracts as a heritable neural basis of social communication deficits in autism spectrum disorder: A sibling study using tract-based automatic analysis. Autism Res 12(2), 225-238.

Lyttelton, O., Boucher, M., Robbins, S., Evans, A., 2007. An unbiased iterative group registration template for cortical surface analysis. Neuroimage 34(4), 1535-1544.

Miller, K.L., Alfaro-Almagro, F., Bangerter, N.K., Thomas, D.L., Yacoub, E., Xu, J., Bartsch, A.J., Jbabdi, S., Sotiropoulos, S.N., Andersson, J.L., Griffanti, L., Douaud, G., Okell, T.W., Weale, P., Dragonu, I., Garratt, S., Hudson, S., Collins, R., Jenkinson, M., Matthews, P.M., Smith, S.M., 2016. Multimodal population brain imaging in the UK Biobank prospective epidemiological study. Nature neuroscience 19(11), 1523-1536.

Mosconi, L., Berti, V., Quinn, C., McHugh, P., Petrongolo, G., Varsavsky, I., Osorio, R.S., Pupi, A., Vallabhajosula, S., Isaacson, R.S., de Leon, M.J., Brinton, R.D., 2017. Sex differences in Alzheimer risk. Neurology 89, 1-9.

Mosconi, L., Rahman, A., Diaz, I., Wu, X., Scheyer, O., Hristov, H.W., Vallabhajosula, S., Isaacson, R.S., de Leon, M.J., Brinton, R.D., 2018. Increased Alzheimer's risk during the menopause transition: A 3-year longitudinal brain imaging study. PloS one 13(12).

Ning, L., Laun, F., Gur, Y., DiBella, E.V., Deslauriers-Gauthier, S., Megherbi, T., Ghosh, A., Zucchelli, M., Menegaz, G., Fick, R., 2015. Sparse Reconstruction Challenge for diffusion MRI: Validation on a physical phantom to determine which acquisition scheme and analysis method to use? Medical image analysis 26(1), 316-331.

Ozarslan, E., Koay, C.G., Shepherd, T.M., Komlosh, M.E., Irfanoglu, M.O., Pierpaoli, C., Basser, P.J., 2013. Mean apparent propagator (MAP) MRI: a novel diffusion imaging method for mapping tissue microstructure. Neuroimage 78, 16-32.

Pakkenberg, B., Gundersen, H.J., 1997. Neocortical neuron number in humans: effect of sex and age. Journal of Comparative Neurology 384, 312-320.

Peper, J.S., van den Heuvel, M.P., Mandl, R.C., Hulshoff Pol, H.E., van Honk, J., 2011. Sex steroids and connectivity in the human brain: a review of neuroimaging studies. Psychoneuroendocrinology 36(8), 1101-1113.

Peters, A., Morrison, J.H., Rosene, D.L., Hyman, B.T., 1998. Feature Article Are Neurons Lost from the Primate Cerebral Cortex during Normal Aging? Cerebral cortex 8, 295-300.

Pfefferbaum, A., Sullivan, E.V., 2015. Cross-sectional versus longitudinal estimates of age-related changes in the adult brain: overlaps and discrepancies. Neurobiology of aging 36(9), 2563-2567.

Ritchie, S.J., Tucker-Drob, E.M., Cox, S.R., Dickie, D.A., Del, C.V.H.M., Corley, J., Royle, N.A., Redmond, P., Munoz Maniega, S., Pattie, A., Aribisala, B.S., Taylor, A.M., Clarke, T.K., Gow, A.J., Starr, J.M., Bastin, M.E., Wardlaw, J.M., Deary, I.J., 2017. Risk and protective factors for structural brain ageing in the eighth decade of life. Brain Struct Funct 222(8), 3477-3490.

Seiler, S., Ropele, S., Schmidt, R., 2014. Magnetization transfer imaging for in vivo detection of microstructural tissue changes in aging and dementia: a short literature review. Journal of Alzheimer's disease : JAD 42 Suppl 3, S229-237.

Seltzer, B., Zolnouni, P., Nunez, M., Goldman, R., Kumar, D., Ieni, J., Richardson, S., Group, D.S., 2004. Efficacy of donepezil in early-stage Alzheimer disease: a randomized placebo-controlled trial. Arch Neurol 61(12), 1852-1856.

Sexton, C.E., Walhovd, K.B., Storsve, A.B., Tamnes, C.K., Westlye, L.T., Johansen-Berg, H., Fjell, A.M., 2014. Accelerated changes in white matter microstructure during aging: a longitudinal diffusion tensor imaging study. The Journal of neuroscience : the official journal of the Society for Neuroscience 34(46), 15425-15436.

Sporns, O., Tononi, G., Kotter, R., 2005. The human connectome: A structural description of the human brain. PLoS computational biology 1(4), e42.

Stadlbauer, A., Salomonowitz, E., Strunk, G., Hammen, T., Ganslandt, O., 2008. Assessment with Diffusion-Tensor Imaging and Quantitative Fiber Tracking. Radiology 247, 179-188.

Sudlow, C., Gallacher, J., Allen, N., Beral, V., Burton, P., Danesh, J., Downey, P., Elliott, P., Green, J., Landray, M., Liu, B., Matthews, P., Ong, G., Pell, J., Silman, A., Young, A., Sprosen, T., Peakman, T., Collins, R., 2015. UK biobank: an open access resource for identifying the causes of a wide range of complex diseases of middle and old age. PLoS Med 12(3), e1001779.

Sullivan, E.V., Adalsteinsson, E., Pfefferbaum, A., 2006. Selective age-related degradation of anterior callosal fiber bundles quantified in vivo with fiber tracking. Cerebral cortex 16, 1030-1039.

Sullivan, E.V., Pfefferbaum, A., 2006. Diffusion tensor imaging and aging. Neuroscience and biobehavioral reviews 30(6), 749-761.

Tian, Q., Glynn, N.W., Erickson, K.I., Aizenstein, H.J., Simonsick, E.M., Yaffe, K., Harris, T.B., Kritchevsky, S.B., Boudreau, R.M., Newman, A.B., Lopez, O.L., Saxton, J., Rosano, C., Health, A.B.C.S., 2015. Objective measures of physical activity, white matter integrity and cognitive status in adults over age 80. Behav Brain Res 284, 51-57.

Tomasi, D., Volkow, N.D., 2012. Laterality patterns of brain functional connectivity: gender effects. Cerebral cortex 22(6), 1455-1462.

Tsai, T.H., Su, H.T., Hsu, Y.C., Shih, Y.C., Chen, C.C., Hu, F.R., Tseng, W.I., 2019. White matter microstructural alterations in amblyopic adults revealed by diffusion spectrum imaging with systematic tract-based automatic analysis. Br J Ophthalmol 103(4), 511-516.

Tuch, D.S., 2004. Q-ball imaging. Magnetic resonance in medicine 52, 1358-1372.

Vinke, E.J., de Groot, M., Venkatraghavan, V., Klein, S., Niessen, W.J., Ikram, M.A., Vernooij, M.W., 2018. Trajectories of imaging markers in brain aging: the Rotterdam Study. Neurobiology of aging 71, 32-40.

Wallace, E.J., Mathias, J.L., Ward, L., 2018. The relationship between diffusion tensor imaging findings and cognitive outcomes following adult traumatic brain injury: A meta-analysis. Neuroscience and biobehavioral reviews 92, 93-103.

Williamson, W., Lewandowski, A.J., Forkert, N.D., Griffanti, L., Okell, T.W., Betts, J., Boardman, H., Siepmann, T., McKean, D., Huckstep, O., Francis, J.M., Neubauer, S., Phellan, R., Jenkinson, M., Doherty, A., Dawes, H., Frangou, E., Malamateniou, C., Foster, C., Leeson, P., 2018. Association of Cardiovascular Risk Factors With MRI Indices of Cerebrovascular Structure and Function and White Matter Hyperintensities in Young Adults. JAMA 320(7), 665-673.

Wu, C.H., Hwang, T.J., Chen, Y.J., Hsu, Y.C., Lo, Y.C., Liu, C.M., Hwu, H.G., Liu, C.C., Hsieh, M.H., Chien, Y.L., Chen, C.M., Isaac Tseng, W.Y., 2015. Primary and secondary alterations of white matter connectivity in schizophrenia: A study on first-episode and chronic patients using whole-brain tractography-based analysis. Schizophr Res 169(1-3), 54-61.

Ycaza Herrera, A., Mather, M., 2015. Actions and interactions of estradiol and glucocorticoids in cognition and the brain: Implications for aging women. Neuroscience and biobehavioral reviews 55, 36-52.

Yeatman, J.D., Wandell, B.A., Mezer, A.A., 2014. Lifespan maturation and degeneration of human brain white matter. Nature communications 5, 4932.

Yoon, B., Shim, Y.S., Lee, K.S., Shon, Y.M., Yang, D.W., 2008. Region-specific changes of cerebral white

matter during normal aging: a diffusion-tensor analysis. Arch Gerontol Geriatr 47(1), 129-138.
Zhang, F., Wu, Y., Norton, I., Rigolo, L., Rathi, Y., Makris, N., O'Donnell, L.J., 2018. An anatomically curated fiber clustering white matter atlas for consistent white matter tract parcellation across the lifespan. Neuroimage 179, 429-447.